

DOI: 10.1002/ ((please add manuscript number))

Article type: Full paper

**Organic gelators as growth control agents for stable and reproducible hybrid
perovskite-based solar cells**

*Sofia Masi,^[a] Aurora Rizzo,^[a] Rahim Munir,^[b] Andrea Listorti,^[a,c] Antonella Giuri,^[d]
Carola Esposito Corcione,^[d] Neil D. Treat,^[e] Giuseppe Gigli,^[a,c] Aram Amassian,^{[b]*} Natalie
Stingelin,^{[e,f]*} and Silvia Colella^{*[a,c]}*

Dr. S. Masi, Dr. A. Rizzo, Dr. A. Listorti, Prof. G. Gigli, Dr. S. Colella

Istituto di Nanotecnologia CNR-Nanotec, Polo di Nanotecnologia c/o Campus Ecotekne, Via
Monteroni 73100 Lecce, Italy

Mr. Munir, Prof. A. Amassian

King Abdullah University of Science and Technology (KAUST), Physical Sciences and
Engineering Division, and, KAUST Solar Center (KSC), Thuwal 23955-6900, Saudi Arabia.

Dr. A. Listorti, Prof. G. Gigli, Dr. S. Colella

Dipartimento di Matematica e Fisica “E. De Giorgi”, Università del Salento, Via per
Arnesano, 73100 Lecce, Italy

Mrs. A. Giuri, Dr. C. Esposito Corcione

Dipartimento di Ingegneria dell’Innovazione, Università del Salento, Via per Arnesano,
73100 Lecce, Italy

Dr. N. D. Treat, Prof. N. Stingelin

Department of Materials & Centre for Plastic Electronics, Imperial College London,

Exhibition Road, London SW7 2AZ, UK

Prof. N. Stingelin

School of Materials Science & Engineering and School of Chemical & Biomolecular

Engineering, Georgia Institute of Technology, 311 Ferst Drive, Atlanta, Georgia 30332, USA

Email: aram.amassian@kaust.edu.sa; silvia.coella@unisalento.it;

natalie.stingelin@mse.gatech.edu

Keywords: halide perovskites, organic gelators, photovoltaics

Low molecular-weight organic gelators are widely used to influence the solidification of polymers, with applications ranging from packaging items, food containers to organic electronic devices, including organic photovoltaics. Here, this concept is extended to hybrid halide perovskite-based materials. In-situ time-resolved grazing incidence wide angle x-ray scattering (GIWAXS) measurements performed during spin-coating reveal that organic gelators beneficially influence the nucleation and growth of the perovskite precursor phase. This can be exploited for the fabrication of planar n-i-p heterojunction devices with MAPbI₃ (MA = CH₃NH₃⁺) that display a performance that not only is enhanced by ~25% compared to solar cells where the active layer was produced without the use of a gelator but that also feature a higher stability to moisture and a reduced hysteresis. Most importantly, the presented approach is straight-forward and simple, and it provides a general method to render the film-formation of hybrid perovskites more reliable and robust, analogous to the control that is afforded by these additives in the processing of commodity ‘plastics’.

1. Introduction

The recent introduction of hybrid organic-inorganic perovskites as solution-processable photoactive component for use in thin-film photovoltaic (PV) devices^[1-4] has galvanized the PV community as it promises to bring to the market a low-cost, high-efficient and versatile thin-film PV technology. Thanks to the eclectic features of hybrid perovskites, various thin-film device layouts have so far been explored with the main emphasis more recently being directed on the design and processing of polycrystalline perovskite-based devices.^[5-9] Thereby, much effort has been focused towards improving the surface coverage of the solution-processed perovskite active layer, *e.g.*, by increasing the size and quality of their crystalline domains^[10-12] The latter was shown to reduce the overall bulk defect density, mitigating recombination, improving charge transport characteristics, and reducing the hysteretic behavior by suppressing ions/carriers trapping during solar cell operation.

Various strategies, such as thermal annealing,^[13,14] additive inclusion,^[15-18] modification of precursor concentrations and carrier solvents^[19,20] and high-temperature-casting^[21] have been investigated so far to control perovskite structure, grain size, degree of crystallinity and stability to moisture – however with varying success.^[21,22] Here, we introduce the use of commercially available, low molecular-weight organic gelators (LMOGs), namely 1,3:2,4-di-O-methylbenzylidene-D-sorbitol (MDBS) and 1,3:2,4-di-O-dimethylbenzylidene-D-sorbitol (DMDBS) (Figure 1), to gain control over the solidification of MAPbI₃ and to establish a means for controlling its structure, properties and stability in the context of perovskite solar cells.

LMOGs are commonly used additives in the commodity plastics area because they promote – already at minute quantities – gelation of polymer solutions or melts upon cooling while they have no effect on these systems at elevated temperatures.^[23] LMOGs are, thus, used in a number of industrial applications,^[23] thanks to their easily tunable molecular structures that makes them compatible with a wide range of plastics. More recently, they proved to be useful in controlling the solidification of organic PV blends and a range of organic semiconductors, small-molecular and polymeric, where they acted as nucleating agent.^[24]

Amongst the plethora of LMOGs that are commercially available, 1,3:2,4-di-O-benzylidene-D-sorbitol (DBS) and its derivatives are some of the most versatile gelators because they feature hydrophobic phenyl rings in combination with polar hydroxyl groups making them compatible with a wide range of materials of varying polarity. The assembly of LMOGs is dynamic and reversible, and it involves the formation of a hydrogen bond network caused by *(i)* the presence of these terminal hydroxyl groups and *(ii)* the specific molecular geometry of DBS derivatives (Figure 1). This assembly promotes the aggregation of nanoscale fibers and the gelation of the solvent that leads to crystal nucleation in many plastics. The question remains, however, whether these useful additives also can be exploited for controlling the solidification of other materials than plastics, including inorganic/organic hybrid materials such as hybrid perovskites.

Here we demonstrate the reproducible fabrication of highly efficient and stable MAPbI₃-based solar cells by introducing a very small quantity of organic gelator as additive to the hybrid perovskite precursor solution. We show that analogous to the use of this additive in combination with the bulk commodity polymer isotactic polypropylene (*i*-PP) or a range of organic semiconductors,^[24] a small quantity of specific LMOGs is sufficient to control the nucleation and solid-state structure formation of the active hybrid perovskite layer, providing a tool to control the resulting solid-state microstructure of the perovskite phase. Using a combination of rheometry data and *in-situ* x-ray diffraction measurements performed during spin-coating of the active layer, we show that one LMOG studied here, *i.e.* MDBS, forms within the precursor solutions a three-dimensional network that is stabilized thanks to very specific and balanced supramolecular interactions of this additive with the precursor solvate phase. This network impacts the polycrystalline film formation of the hybrid perovskite, leading to a very compact array of crystalline domains. Noticeably, addition of MDBS seems to lead to the formation of a thermodynamically more stable perovskite thin-film structure, as our thermal analysis data indicates. Device performance is thereby not compromised: planar *n-i-p* heterojunction devices prepared with MAPbI₃ and MDBS display increased device performance from 11.5% (reference device without additive) to 14.5% (with MDBS). In addition, a notably decreased device-to-device performance variation and a reduced hysteresis is observed for the devices comprising the LMOG. As importantly, the introduction of a small amount of LMOG lowers the crystallization temperature of the perovskite system to below 100°C which assist controlling the solidification processes. Also, the stability to moisture seems to increase. These features combined with the relatively high photovoltaic efficiency make the use of LMOGs a simple and effective method foreseeing relevant industrial applications of perovskite solar cells.

2. Results and discussion

Methyl-substituted derivatives of DBS are frequently used to gel polar aprotic solvents. Hence, we selected two common DBS derivatives – *i.e.* MDBS and DMDBS – as they can be dissolved into solvent systems such as 2:1 γ -butyrolactone-dimethylsulfoxide (γ BL-DMSO), often used to deposit the MAPbI₃ precursor. Since MDBS and DMDBS are slightly apolar, their solubility in γ BL-DMSO especially at lower temperatures is, however, somewhat limited. This ensures that the solvent mixture can be gelled.^[25] We first tested the gelling ability of either DBS derivative by adding 0.1 wt%, 0.5 wt% or 1 wt% of these LMOGs to γ BL-DMSO, followed by heating these mixtures to 125 °C while stirring until clear solutions were obtained. Cooling these solutions to room temperature, we find that MDBS forms a relatively weak gel, while DMDBS forms a mechanically more stable gel (Figure. S1a, Supporting Information). When the LMOGs were added to perovskite precursor (PbI₂ + MAI) solutions, using again different LMOG concentrations (0.1 wt%, 0.5 wt% or 1 wt%), beneficially, no immediate gel formation was found to occur after cooling. Also, the cooled solutions appeared to be of lower viscosities compared to systems where no perovskite precursor had been added. We attribute this behavior to the fact that the gelation behavior of LMOGs in a complex environment of solvated salts often is different when compared to a scenario where they are used in a solvent system without salts.^[25] This could be a beneficial finding when formulating ‘inks’ that are compatible with solution-based coating and manufacturing methodologies as undesirable, early-stage gelation can be prevented.^[23]

To quantify the above observations and to obtain further information on the potential network formation of the LMOGs and how this changes the interplay between the solvent molecules and the MAPbI₃ precursors,^[26,27] we measured the variation of the complex viscosity (η^*) of MAPbI₃, MAPbI₃-MDBS and MAPbI₃-DMDBS solutions with frequency (Figure 2a), as well as their frequency-dependent storage (G') and loss (G'') moduli (Figure 2b-d). We observe that

the addition of DBS derivatives to the MAPbI₃ solutions significantly increases their complex viscosity in the frequency range analyzed, supporting our visual observations that the LMOGs have a notable gelating ability on the perovskite solutions. We attribute this fluid dynamical behavior to the well-known tendency of sorbitol derivatives to form a nanofibrillar network in a range of solvents,^[23] as schematically depicted in Figure 1a.

More insights can be gained when comparing the storage and loss moduli of the pristine perovskite precursor solution with solutions containing MDBS or DMDBS (Figure 2b-d). For the pristine solution, the loss modulus G'' exceeds the storage modulus G' over most of the frequency range that we measured. Moreover, both moduli strongly vary with frequency. This response indicates that the MAPbI₃ solution behaves as a low viscosity liquid,^[28] which is in agreement with our visual observations that these solutions were free-flowing. In strong contrast, the MDBS and DMDBS solutions show gel-like responses: G' is larger than G'' over the entire range of frequencies investigated here, indicating a dominant elastic behavior. Moreover, their moduli are relatively frequency-independent, reflecting the presence of a network structure that is invariant (non-relaxing) over long time scales.^[28] Comparing the moduli of the perovskite solutions containing MDBS or DMDBS to the corresponding solutions comprising only the LMOGs (Figure S2), we find that both the G' and G'' moduli are higher for the MDBS-MAPbI₃ solutions compared to the solution comprising only MDBS. Clearly, while MAPbI₃ by itself is not a gelator for γ BL-DMSO, it appears to synergistically strengthen the MDBS elastic network suggesting that possibly some interactions between this organic gelator and the perovskite precursor exist. In contrast, for DMDBS solutions (with and without perovskite precursor) the opposite is observed; i.e. the G' and G'' moduli are lower for the LMOG-MAPbI₃ solutions compared to the solution comprising DMDBS only. We attribute this to the limited solubility of DMDBS in the solvent mixture and the reduced interaction of the LMOG with the inorganic species in these solutions. The latter likely is caused by the fact that this additive features rather apolar methyl groups with which neither the solvent molecules nor

the perovskite precursor can strongly interact.^[29] Such a picture is supported by scanning electron microscopy (SEM) data on films prepared from precursor solutions comprising DMDBS as the LMOG (Figure S1b). We observe micron-scale crystals of DMDBS segregated from the perovskite component which can only occur when there are limited interactions between the different species. Such a morphology, not surprisingly, leads to poor devices performance (Table S1).

In order to better understand the solid-state microstructure formation especially of the MDDBS systems, where a certain interplay between the additive and the precursor exists, we went on to conduct in-situ time-resolved grazing-incidence wide-angle x-ray scattering (GIWAXS) measurements, uniquely performed during spin-coating of the perovskite formulations with and without organic gelators onto compact TiO₂. An optimized solvent-engineering method was used, consisting of a two-step spin-coating process performed at different speeds (see experimental section for details) followed by dichloromethane (DCM) onto the drying layers to promote the formation of a precursor film. These can subsequently be thermally converted and crystallized into a uniform and smooth polycrystalline film.^[30-32]

In-situ GIWAXS measurements were used to follow the precursor film evolution through all the phases of the multi-step method we used. In Figure S3, we show representative two-dimensional GIWAXS images taken at critical times ($t = 15, 30, 45$ and 90 s) after initiating the spin-coating of the different solutions, highlighting the state of the sample at different moments. We first discuss pristine solutions comprising no additives to highlight certain specific features of the development of perovskite thin films when deposited from solution. Specifically, the data taken at $t = 15$ and 30 s show evidence of a disordered precursor phase formation ($q < 6 \text{ nm}^{-1}$) which subsequently crystallizes ($t = 45$ and 90 s) as indicated by formation of diffraction rings at $q = 4.7 \text{ nm}^{-1}$, 5.2 nm^{-1} and 6.6 nm^{-1} . Weak scattering features are also visible at $q = 9.4 \text{ nm}^{-1}$ and 10.3 nm^{-1} , corresponding, respectively, to PbI₂ and perovskite diffractions.^[33,34]

We also traced the time evolution of these various features using solutions of different additive content azimuthally integrating (see Figure S4) each GIWAXS snapshot taken with a time-resolution of 400 ms. We plot the 2D-intensity maps in Figures 3a, b and c, respectively, pristine, 0.1 wt% and 0.5 wt% MDDBS/perovskite precursors solutions. The x-axis represents the time scale, the y-scale represents q (radial), and the z-scale is representative of intensity. Individual q -plots taken at $t = 15, 30, 45$ and 90 s, respectively, are also shown in Figures 3d-g with the insets of (e)-(g) focusing on the $8 < q < 11 \text{ nm}^{-1}$ range. Having a close look at the data for the sample comprising no LMOG, we observe a broad scattering feature ($q < 6 \text{ nm}^{-1}$; peak $\sim 3.5 \text{ nm}^{-1}$) which dynamically evolves during the initial 40 s of spin-coating, subsequently forming sharp scattering features ($q = 4.7, 5.2$ and 6.6 nm^{-1}) that can be assigned to a crystalline precursor solvate that starts to form even prior to DCM drip. This disordered precursor phase is believed to be a sol-gel precursor phase with mesoscale order; its development is accompanied with the formation of lead iodide and perovskite phases, for which low-intensity peaks are visible in Figure 3a and 3f. The integrated intensities and FWHM of the diffraction features are summarized in Table 1.

For samples comprising MDDBS, we find that in systems comprising 0.1 wt% of this additive, precursor crystallization occurs ~ 50 s after the initial spin-coating process (*i.e.* post-DCM drip); this is ~ 25 s later to when this process starts when 0.5 wt% MDDBS is added. In this scenario, crystallization occurs only ~ 25 s after the spin-coating that is well before the DCM drip. [NB. For systems not comprising any LMOG crystallization on-set of crystallization is found to be around ~ 40 s.] Clearly the addition of 0.1 wt% MDDBS promotes formation of a disordered precursor phase and enhances this phase's longevity as compared with the pristine formulations. Increasing the amount of MDDBS to 0.5 wt% hinders formation of this disordered precursor phase and leads to an early onset of the precursor solvate crystallization. Since the state of the PbI_2 and perovskite phases appears to be linked to the fate of the precursor solvate

crystallization and whether it occurs post-drip (as in 0.1 wt% -MDBS formulations) or pre-drip (as in the 0.5 wt%-MDBS formulations) we deeper analyzed the scattering features of the various films at 90 s (Figure 5g, Table 1). The as-cast films formed using 0.1 wt% MDBS have sharper MAPbI₃ diffraction features than the other samples, as well as the sharpest precursor solvate diffraction features. The perovskite peak in the as-cast samples comprising 0.1 wt% MDBS shows the lowest FWHM of 0.38 nm⁻¹ compared with 0.54 nm⁻¹ for films cast from pristine precursor solutions and 0.7 nm⁻¹ for samples with 0.5 wt% MDBS. This finding suggests that addition of an optimum amount of MDBS leads not only to more homogenous structures with respect to grain size but also the smallest grains. In fact, all other diffractions features display the lowest FWHM in systems comprising 0.1wt% MDBS.

The importance of what type of precursor solvate phase forms in as-cast films stems from the fact that this seems to determine the final microstructure and morphology of the polycrystalline perovskite film that develops during annealing/precursor conversion. We scrutinized this hypothesis further conducting annealing experiments. We find that when heating thin films produced from the various solutions investigated here to 100 °C under N₂, a striking difference in microstructure can be observed between perovskite films produced from pristine solutions and those comprising, respectively, 0.1 and 0.5 wt% of MDBS (Figure 4).

Upon heating, the additives show a strong tendency to crystallize into fibrillar structures (as reported before, see Ref. 29) even in presence of the perovskite precursors. These structures seem to induce the crystallization process of the perovskite phase at lower temperature compared to samples where no LMOG was added: at 60°C for perovskite/0.1 wt%-MDBS structures and at 40°C for perovskite/0.5 wt%-MDBS films. These observations agree with the evolution of the storage modulus G' with temperature (see Figure S5), which relatively rapidly increases at temperatures above 60 °C for systems to which LMOGs were added, while for the pristine perovskite precursors solution a steep increase of G' (which we attribute to crystallization) occurs only at temperatures > 80 °C. This suggests that additive affects the

nucleation/assembly-process of the perovskite species through gel-network formation,^[29] allowing the crystallization of perovskites to occur at lower temperatures.

This finding is supported by differential scanning calorimetry (DSC) measurements on the different precursors solutions. Figure 5a shows the DSC heating thermograms measured at 10°C/min, where the endotherm related to solvent evaporation has been subtracted in order to isolate the perovskite crystallization exotherm. While we find noticeable crystallization exotherms both for the neat MAPbI₃ and MAPbI₃/0.1 wt%-LMGO systems, this features displays a somewhat earlier onset (see Table S1) and is somewhat more pronounced when MDBS was used as the additive.

Deducing the crystallization enthalpy ΔH_c from the area of the respective exotherms (based on an extrapolated horizontal baseline aligned to the asymptotic value of the DSC signal at the end of the reaction), for different heating rates, we find that ΔH_c for MAPbI₃/0.1 wt%-MDBS is significantly higher than for MAPbI₃ (respectively, -115 ± 1 kJ/mol and -82 ± 4 kJ/mol – see Figure 5b and Table S2). This indicates that independent of heating rate, crystalline films of a higher degree of crystallinity are realized when using the MDBS additive. It also suggests that more stable structures are produced. In fact, a higher enthalpy measured for the perovskite formation process: $\text{PbI}_2 + \text{MAI} \rightarrow \text{MAPbI}_3$, has previously been attributed to be a sign for the development of a more stable perovskite structure.^[35,36] The reason is that a higher enthalpy gain leads to a higher thermodynamic stability of the resulting perovskite compound.^[37] The lower standard deviation found for ΔH_c for system with MDBS (Table S1) is in addition is a sign for a more reproducible crystallization process.

Introduction of MDBS has additional benefits. The narrower grain size distribution and the smaller grain size that seems to be realizable in systems comprising this LMOG according to our X-ray data (smaller FWHM) and that likely is a direct consequence of the nucleation effect of MDBS on the perovskite precursor, appears to lead to less light scattering. In addition, the

presence of MDBS also leads to the formation of a more compact film (Figure 6a), both effects contributing to a two-fold increase of the MAPbI₃/0.1 wt%-MDBS film absorption in the UV-visible wavelength regime compared to films prepared without additives of comparable thickness (160 nm; see Figure 6b). This should affect the light-harvesting capability of devices prepared with such structures.

An enhanced moisture resistance compared to samples prepared without LMGs is also observed. Exposing perovskite films produced from a pristine precursor solution as well as samples where 0.1 wt% MDBS was added to 70% relative humidity (room temperature; ambient air) for 15 days, we observe a severe degradation of perovskite structure without additives. This is reflected in the significant increase in intensity of the (001) PbI₂ diffraction measured in WAXS (Figure S6), which becomes comparable to the (110) MAPbI₃ reflection at 14.08°. In contrast, the aged MAPbI₃/0.1 wt%-MDBS films display a PbI₂ diffraction of rather low intensity, implying a much lower degree of decomposition. This reduced moisture sensitivity of the latter samples likely is a direct consequence of (i) the more stable energy state of MAPbI₃ structures produced with MDBS as additive (see Figure 5b), and (ii) the formation of a more compact film (Figure 6a) that make the polycrystalline film less accessible to hydration/decomposition reactions and to the infiltration of moisture.

As already briefly alluded to above, the presence of MDBS – perhaps not surprisingly – strongly affects the properties and performance of perovskite-based solar cells. Our results are summarized in Table 2 and Figure 6c where we also present a schematic illustration of the planar FTO-TiO₂-perovskite/MDBS (160 nm)-spiro-MeOTAD (200 nm)/Au device architecture we utilized here. Immediate observations that can be made are: (i) the PCE increases from 11.5 % for devices prepared without gelator to 14.5 % for cells comprising 0.1 wt% MDBS. (ii) Devices where MDBS was introduced display a significantly reduced hysteresis (Table S3). (iii) The reproducibility of device performances increases when this LMOG was used for their fabrication. Indeed, we find a very small device-to-device standard

deviation (0.5%) which is drastically lower than what we observe for cells prepared from pristine solutions (1.6%; see Figure S7).

This superior photovoltaic performance that is observed for the devices from solutions comprising the additive, on the one hand, can be attributed to the formation of a very dense perovskite layer caused by the presences of MDDBS (Figure 6a). This can have a few likely benefits: such a dense active layers can prevent undesirable recombination processes that occur through direct contact between TiO_2 and a hole transporting layer; it, thus, assists in increasing the charge collection efficiency and the fill factor, FF. On the other hand, enhancing the light-harvesting capacity of the active layer has a direct impact on the extracted current, resulting also in an average improvement in the power conversion efficiency. (Figure 6c; Table 2) It is worth noting in this context that the thicknesses of the MAPbI_3 layers with and without MDDBS were comparable (160 ± 10 nm; Figure 6d).

We seem also to learn about the structural requirements that lead to optimum device performance. For instance, we find that pristine MAPbI_3 annealed for 10 minutes at 100°C presents the same PV performance of $\text{MAPbI}_3/0.1$ wt%-MDDBS system annealed for half of the time (5 minutes) at the same temperature (Figure S8a), likely owing to the earlier occurring of crystallization in the presence of MDDBS. However, best solar cells for both systems are obtained with films annealed for 10 minutes (Figure 6c). These conditions lead to perovskite/MDDBS-based films that still contain a small amount of PbI_2 (Figure S8b). The presence of some PbI_2 may be beneficial because it might passivate the thin-film architecture. Previous reports have, for instance, shown that upon thermal annealing, PbI_2 species can be preferentially confined at the grain boundaries of thin-film structures leading to successful passivation of them. This assists in controlling the carrier behavior along the heterojunction. Moreover, it will allow to substantially shorten currently used annealing protocols.^[38]

Finally, we verified the performance of devices prepared with various content of MDDBS. The best performance is observed for cells comprising 0.1 wt% MDDBS – *i.e.* a very minute amount, while higher contents of MDDBS leads to performance degradation even though the additive still strongly influences the nucleation and growth of the perovskite phase. Clearly, an optimum can be realized where the additive produces ideal supramolecular assemblies^[29,39] for templating perovskite crystals growth, whereas at higher MDDBS content more branched and less oriented structures appear to form within the perovskite film.

3. Conclusion

We demonstrated that commercially available organic gelators can be successfully used to control the crystallization process of perovskite precursor solutions and films through the formation of a fibrillary 3D-network. This network affects the crystallization thermodynamics of the precursor species and assists in lowering its crystallization temperature. It also renders perovskite formation more stable. Moreover, the presence of an optimal (minute) amount of MDDBS (0.1 wt%) delays the formation of the precursor solvate, but results in a highly crystalline precursor phase. In contrast, too much of the additive accelerates precursor solvate formation which seems to be undesirable for creating highly crystalline structures. Subsequent annealing converts the solvated film into structures comprised of the perovskite phase. Intriguingly the gel-like material created through use of LMOGs enables the formation of more compact films when flat TiO₂ was used as substrate. This appears to make the perovskite drastically more robust towards exposure to moisture. The impact on the crystallization process has also important implications for device fabrication, where the use of organic gelators in future may assist in shortening the thermal annealing protocol. This could become beneficial when going to larger-scale device processing. These benefits come without compromising device performance. Indeed, we demonstrate that the use of MDDBS improves the PCE of planar solar cells from 11.5% to 14.5%, while also a dramatically reduced hysteresis is observed for

the systems that comprise the additive. Clearly, our approach allows at the same time to *i*) achieve very small device-to-device standard deviations, *ii*) improve stability to moisture of the final material compared to systems where no LMOG was added, *iii*) reduce hysteresis for planar *n-i-p* solar cells, and *iv*) lower the crystallization temperature below 100 °C. Our findings, thus, suggest that the use of LMOGs during the processing of perovskite-based materials can be a simple and effective method towards the robust and reliable fabrication of perovskite solar cells.

4. Experimental Section

Materials. All materials were purchased and used as received. Spiro-MeOTAD was purchased from Lumtec and PbI₂, Lead (II) iodide ultra-dry 99.999% (metals basis), from Alfa Aesar. CH₃NH₃I (MAI) was synthesized according to a reported procedure.⁴ CH₃NH₃ (27.86 ml, 40% in methanol, TCI) and hydroiodic acid (30 ml, 57 wt% in water, Aldrich) were mixed at 0 °C and stirred for 2 h. The precipitate was recovered by evaporation at 50 °C for 1 h. The product was washed with diethyl ether three times and finally dried at 60 °C in a vacuum oven for 24 h. 1,3:2,4-di-O-methyl-benzylidene-D-sorbitol(MDBS, Millad 3940) and 1,3:2,4-bis(3,4-dimethyldibenzylidene)sorbitol (DMDBS, Millad 3988).

Optical microscopy. Perovskite solution with and without nucleating agents was prepared and stirred for 2 h at 90 °C before use. These stock solutions were coated onto bl-TiO₂/FTO substrate by a consecutive two-step spin-coating process at 1,000 and 4,000 r.p.m for 10 and 60 s, respectively with a dipping of dichloromethane at 10 sec to the end with a final film thickness of approximately 160 nm. They were annealed at various temperatures in a nitrogen environment.

Rheological analysis. Dynamic rheological experiments were performed on an Anton Paar Physica MCR 301 instrument equipped with measuring cone plate geometry (CP25-1 with 24.980 mm diameter and angle 1°). Dynamic frequency spectra were conducted in the linear viscoelastic regime of the samples, as determined from dynamic stress sweep measurements.

Dynamic stress sweeps were conducted at a constant frequency of 1 Hz. The viscosities of the solutions were measured in the low shear rate range ($\omega = 0.01$ -600 rad/s) at 20 °C.

SEM. The SEM imaging was performed by the MERLIN Zeiss SEM FEG instrument at an accelerating voltage of 5 kV, using an In-lens detector.

DSC analysis. Dynamic DSC scans were performed on perovskite precursors solutions by a differential scanning calorimeter (DSC Mettler Toledo 622). About 6 μ l of liquid samples were put into opened aluminum flat disks and heated from 20 up to 200 °C at different scan rate (0.5, 2, 5, 10 °C/min) under nitrogen atmosphere flow at 60 mL/min.

XRD. The XRD spectra of the prepared films were measured with a PAN analytical X'Pert-PRO Materials Research Diffractometer using graphite-monochromated Cu K α radiation ($\lambda = 1.5405$ Å).

GIWAXS The in situ GIWAXS experiments were conducted in ambient environment (R.H. ~20%) at D1 beam line at the Cornell High Energy Synchrotron Source (CHESS). For spin coating, a custom-built spin coater was used with kapton tape as a protection from solution splashing. A Pilatus 200K area detector was used as the detector. The exposure time was set to 0.4 s. The anti-solvent drip was performed remotely from outside the hutch.

Device fabrication and characterization. Glass substrates (Viontech) and FTO-coated glass substrates (Solaronix) were cleaned by ultrasonication in a deionized water, 2-propanol and acetone. Substrates were treated to the TL1-washing procedure (washed in double distilled water (Milli-Q water), hydrogen-peroxide (H₂O₂) and ammonia (NH₃) 5:1:1 v/v (at 80°C for 10 minutes) to remove organic contamination, then rinsed ten times in water prior next depositions. A 80 nm-thick TiO₂ dense hole-blocking layer (ETL) was deposited on glass/FTO by spin coating two times at 3,000 rpm for 60 sec and annealed at 125°C using a commercial titanium diisopropoxidebis(acetylacetonate) solution (75% in 2-propanol, Sigma-Aldrich) diluted in butanol (0,15M) for 10 minutes and one time at 3,000 rpm for 60 sec and annealed at

520 °C using a commercial titanium diisopropoxidebis(acetylacetonate) solution (75% in 2-propanol, Sigma-Aldrich) diluted in butanol (0,3M). The prepared MAI and commercial ultra-dry PbI₂, Alfa Aesar, were stirred (ratio 1:1) in a mixture of γ -butyrolactone (γ BL) and DMSO (2:1vol/vol; γ BL, \geq 99%; DMSO, 99.8%; Sigma-Aldrich) at 60 °C for 12 h, to obtain a 40 wt% solution. The perovskite precursor solution containing MDBS or DMDBS were prepared by adding 0.1 wt%, 0.5 wt% or 1 wt% of either DBS derivative (with respect to MAI+PbI₂ weight) to 40 wt% perovskite precursors solution, followed by heating these mixtures to 125 °C while stirring until clear solutions were obtained. Solutions were then allowed to cool to room temperature. Both pristine perovskite precursor solution and the once containing DBS derivatives were coated onto either glass or TiO₂/FTO substrate by a consecutive two-step spin-coating process at 1,000 and 4,000 r.p.m for 20 and 60 s, respectively with a dripping of dichloromethane at 10 sec to the end. After spin-coating, the films were annealed on a hotplate at 100 °C for 10 min. After cooling to room temperature, a spiro-MeOTAD solution was spin-coated on the perovskite layer at 2,500 r.p.m. for 45 s. Spiro-MeOTAD solution was prepared by dissolving 90 mg of spiro-MeOTAD in 1 ml chlorobenzene (99.8%, Sigma Aldrich), to which were added 28.8 μ l of 4-tert-butylpyridine (96%, Sigma-Aldrich), 17.5 μ l lithium bis(trifluoromethanesulfonyl)imide (LiTFSI) solution (520 mg LI-TSFI in 1 ml acetonitrile, 99.8%, Sigma-Aldrich). This fabrication process was carried out under controlled conditions in a glove-box atmosphere and a temperature between 20 and 25 °C. Finally, 80 nm gold was thermally evaporated on top of the device at a pressure of 5×10^{-6} mbar to form the back contact. The active area of the complete device was 0.09 cm⁻². The devices were characterized after 3h exposure to ambient conditions using a Keithley 2400 Source Measure Unit and AirMass 1.5 Global (AM 1.5G) solar simulator (Newport 91160A) with an irradiation intensity of 100 mW/cm². The solar simulator irradiance was set to 100 mW/cm² using a thermopile radiant power meter with fused-silica window (Spectra Physics Oriel, model 70260). All devices are tested using 100 ms delay time.

Supporting Information

Supporting Information is available from the Wiley Online Library or from the author.

Acknowledgements

S.C. and A.L. acknowledge Regione Puglia and ARTI for funding FIR – future in research projects “PeroFlex” project no. LSBC6N4 and “HyLight” project no. GOWMB21. The authors acknowledge the project Progetto di ricerca PON MAAT (Project Number: PON02_00563_3316357) and PERSEO-“PERovskite-based Solar cells: towards high Efficiency and lOng-term stability” (Bando PRIN 2015-Italian Ministry of University and Scientific Research (MIUR) Decreto Direttoriale 4 novembre 2015 n. 2488, project number 20155LECAJ) for funding. A.R. and S.M. gratefully acknowledge SIR project “Two-Dimensional Colloidal Metal Dichalcogenides based Energy-Conversion Photovoltaics” (2D ECO), Bando SIR (Scientific Independence of young Researchers) 2014 MIUR Decreto Direttoriale 23 gennaio 2014 no. 197 (project number RBSI14FYVD, CUP: B82I15000950008) for funding. The authors acknowledge Sonia Carallo for technical support. N. D. T. acknowledges support from the National Science Foundation’s International Research Fellowship Program (OISE-1201915) and the European Research Council’s Marie Curie International Incoming Fellowship under grant agreement number 300091. N. S. is by a European Research Council Starting Independent Researcher Fellowship under grant agreement number 279587.

Received: ((will be filled in by the editorial staff))

Revised: ((will be filled in by the editorial staff))

Published online: ((will be filled in by the editorial staff))

References

- [1] J. Burschka, N. Pellet, S.-J Moon, R. Humphry-Baker, P. Gao, M. K., Nazeeruddin, M. Gratzel, *Nature* **2013**, 499 (7458), 316-319.
- [2] S. Ryu, J. H. Noh, N. J. Jeon, Y. Chan Kim, W. S. Yang, J. Seo, S. I. Seok, *Energy & Environmental Science* **2014**, 7 (8), 2614-2618.
- [3] W. S. Yang, J. H. Noh, N. J. Jeon, Y. C. Kim, S. Ryu, J. Seo, S. I. Seok, *Science* **2015**, 438, 1234-1237.

- [4] M. M. Lee, J. Teuscher, T. Miyasaka, T. N. Murakami, H. J. Snaith, *Science* **2012**, 338 (6107), 643-647.
- [5] H. Zhou, Q. Chen, G. Li, S. Luo, T.-b. Song, H.-S. Duan, Z. Hong, J. You, Y. Liu, Y. Yang, *Science* **2014**, 345 (6196), 542-546.
- [6] V. L. P. Guerra, D. Altamura, V. Trifiletti, S. Colella, A. Listorti, R. Giannuzzi, G. Pellegrino, G. G. Condorelli, C. Giannini, G. Gigli, A. Rizzo, *J. Mat. Chem. A* **2015**, 3, 20811-20818.
- [7] S. Colella, E. Mosconi, G. Pellegrino, A. Alberti, V. L. P. Guerra, S. Masi, A. Listorti, A. Rizzo, G. G. Condorelli, F. De Angelis, G. Gigli, *J. Phys. Chem. Lett.*, **2014**, 5 (20), 3532-3538.
- [8] A. Genco, F. Mariano, S. Carallo, V. L. P. Guerra, S. Gambino, D. Simeone, A. Listorti, S. Colella, G. Gigli, M. Mazzeo, *Advanced Electronic Materials*, **2016**, DOI:10.1002/aelm.201500325.
- [9] S. Colella, M. Mazzeo, A. Rizzo, G. Gigli, A. Listorti, *The Journal of Physical Chemistry Letters*, **2016**, 7 (21), 4322-4334.
- [10] M. Xiao, F. Huang, W. Huang, Y. Dkhissi, Y. Zhu, J. Etheridge, A. Gray-Weale, U. Bach, Y.-B. Cheng, L., A Spiccia, *Angewandte Chemie International Edition* **2014**, 53 (37), 9898-9903.
- [11] N. J. Jeon, J. H. Noh, W. S. Yang, Y. C. Kim, S. Ryu, J. Seo, S. I. Seok, *Nature* **2015**, 517 (7535), 476-480.
- [12] H. D. Kim, H. Ohkita, H. Benten, S. Ito, *Advanced Materials* **2015**, DOI:10.1002/adma.201504144.
- [13] B. Conings, L. Baeten, C. De Dobbelaere, J. D'Haen, J. Manca, H.-G. Boyen, *Advanced Materials* **2014**, 26 (13), 2041-2046.
- [14] A. Dualeh, N. Tétreault, T. Moehl, P. Gao, M. K. Nazeeruddin, M. Grätzel, *Advanced Functional Materials* **2014**, 24 (21), 3250-3258.

- [15] S. Masi, S. Colella, A. Listorti, V. Roiati, A. Liscio, V. Palermo, A. Rizzo, G. Gigli, *Scientific Reports* **2015**, *5*, 7725.
- [16] P.-W. Liang, C.-Y., Liao, C.-C. Chueh, F. Zuo, S. T. Williams, X.-K. Xin, J. Lin, A. K. Y. Jen, *Advanced Materials* **2014**, *26* (22), 3748-3754.
- [17] C. Zuo, L. Ding, *Nanoscale* **2014**, *6* (17), 9935-9938.
- [18] S. Masi, A. Rizzo, F. Aiello, F. Balzano, G. Uccello-Barretta, A. Listorti, G. Gigli, S. Colella, *Nanoscale*, **2015**, *7*, 18956-18963.
- [19] Q. Wang, Y. Shao, Q. Dong, Z. Xiao, Y. Yuan, J. Huang, *Energy & Environmental Science* **2014**, *7* (7), 2359-2365.
- [20] H.-B. Kim, H. Choi, J. Jeong, S. Kim, B. Walker, S. Song, J. Y. Kim, *Nanoscale* **2014**, *6* (12), 6679-6683.
- [21] W. Nie, H. Tsai, R. Asadpour, J.-C. Blancon, A. J. Neukirch, G. Gupta, J. J. Crochet, M. Chhowalla, S. Tretiak, M. A. Alam, H.-L. Wang, A. D. Mohite, *Science* **2015**, *347* (6221), 522-525.
- [22] X. Li, M. Ibrahim Dar, C. Yi, J. Luo, M. Tschumi, S. M. Zakeeruddin, M. K. Nazeeruddin, H. Han, M. Grätzel, *Nat Chem* **2015**, *7* (9), 703-711.
- [23] N. Mohmeyer, P. Wang, H.-W. Schmidt, S. M. Zakeeruddin, M. Gratzel, *Journal of Materials Chemistry* **2004**, *14* (12), 1905-1909.
- [24] N. D. Treat, J. A. Nekuda Malik, O. Reid, L. Yu, C. G. Shuttle, G. Rumbles, C. J. Hawker, M. L. Chabynyc, P. Smith, N. Stingelin, *Nat Mater* **2013**, *12* (7), 628-633.
- [25] J. Li, K. Fan, L. Niu, Y. Li, J. Song, *The Journal of Physical Chemistry B* **2013**, *117* (19), 5989-5995.
- [26] Y. Zhao, K. Zhu, *The Journal of Physical Chemistry C* **2014**, *118* (18), 9412-9418.
- [27] G. E. Eperon, V. M. Burlakov, P. Docampo, A. Goriely, H. J. Snaith, *Advanced Functional Materials* **2014**, *24* (1), 151-157.
- [28] A. Y. Malkin, *Journal of Non-Newtonian Fluid Mechanics* **2013**, *192*, 48-65.

- [29] B. O. Okesola, V. M. P. Vieira, D. J. Cornwell, N. K. Whitelaw, D. K., Smith, *Soft Matter* **2015**, *11* (24), 4768-4787.
- [30] V. Trifiletti, N. Manfredi, A. Listorti, D. Altamura, C. Giannini, S. Colella, G. Gigli, A. Rizzo, *Adv. Mat. Interface*, **2016**, DOI:10.1002/admi.201600493.
- [31] A. Giuri, S. Masi, S. Colella, A. Kovtun, S. Dell'Elce, E. Treossi, A. Liscio, C. Esposito Corcione, A. Rizzo, A. Listorti, *Adv. Funct. Mat*, **2016**, DOI:10.1002/adfm.201603023.
- [32] T. Miletić, E. Pavoni, V. Trifiletti, A. Rizzo, A. Listorti, S. Colella, N. Armaroli, D. Bonifazi, *ACS Applied Materials & Interfaces*, **2016**, *8*, 27966-27973.
- [33] Y.-C. Huang, C.-S. Tsao, Y.-J. Cho, K.-C. Chen, K.-M. Chiang, S.-Y. Hsiao, C.-W. Chen, C.-J. Su, U. S. Jeng, H.-W. Lin, *Scientific Reports* **2015**, *5*, 13657.
- [34] K. W. Tan, D. T. Moore, M. Saliba, H. Sai, L. A. Estroff, T. Hanrath, H. J. Snaith, U. Wiesner, *ACS Nano* **2014**, *8* (5), 4730-4739.
- [35] A. Buin, P. Pietsch, J. Xu, O. Voznyy, A. H. Ip, R. Comin, E. H. Sargent, *Nano Letters* **2014**, *14* (11), 6281-6286.
- [36] J. Haruyama, K. Sodeyama, L. Han, Y. Tateyama, *The Journal of Physical Chemistry Letters* **2014**, *5* (16), 2903-2909.
- [37] A. Buin, R. Comin, J. Xu, A. H. Ip, E. H. Sargent, *Chemistry of Materials* **2015**, *27* (12), 4405-4412.
- [38] Y. H. Lee, J. Luo, R. Humphry-Baker, P. Gao, M. Grätzel, M. K. Nazeeruddin, *Advanced Functional Materials* **2015**, *25* (25), 3925-3933.
- [39] J. Lipp, M. Shuster, G. Feldman, Y. Cohen, *Macromolecules* **2008**, *41* (1), 136-140.

Figure 1. Schematic illustration of the supramolecular assemblies that seem to form within the perovskite precursor solutions between the inorganic component and the organic gelator molecules such as MDBS and DMDBS used in this study.

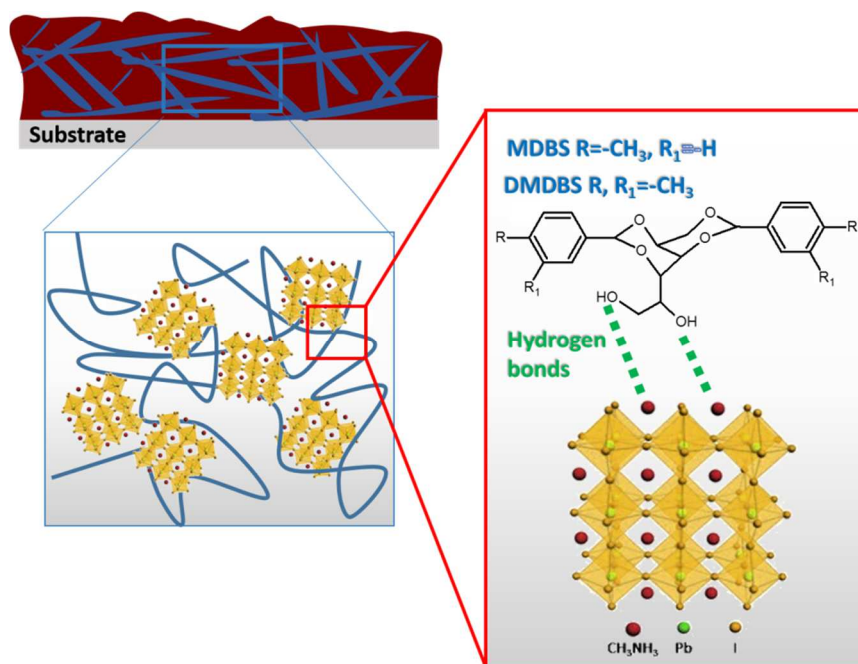


Figure 2. (a) Complex viscosity of perovskite precursor solutions to which 0.1 wt% MDBS, or 0.1 wt% DMDBS was added. Data for the pristine precursor solution is also shown. (b,c). Comparison of the storage (G') and loss modulus (G'') profile versus frequency for different perovskite precursor solutions: (b) pristine perovskite precursor solution; (c) precursor solution comprising 0.1 wt% MDBS, and (d) precursor solution comprising 0.1 wt% DMDBS.

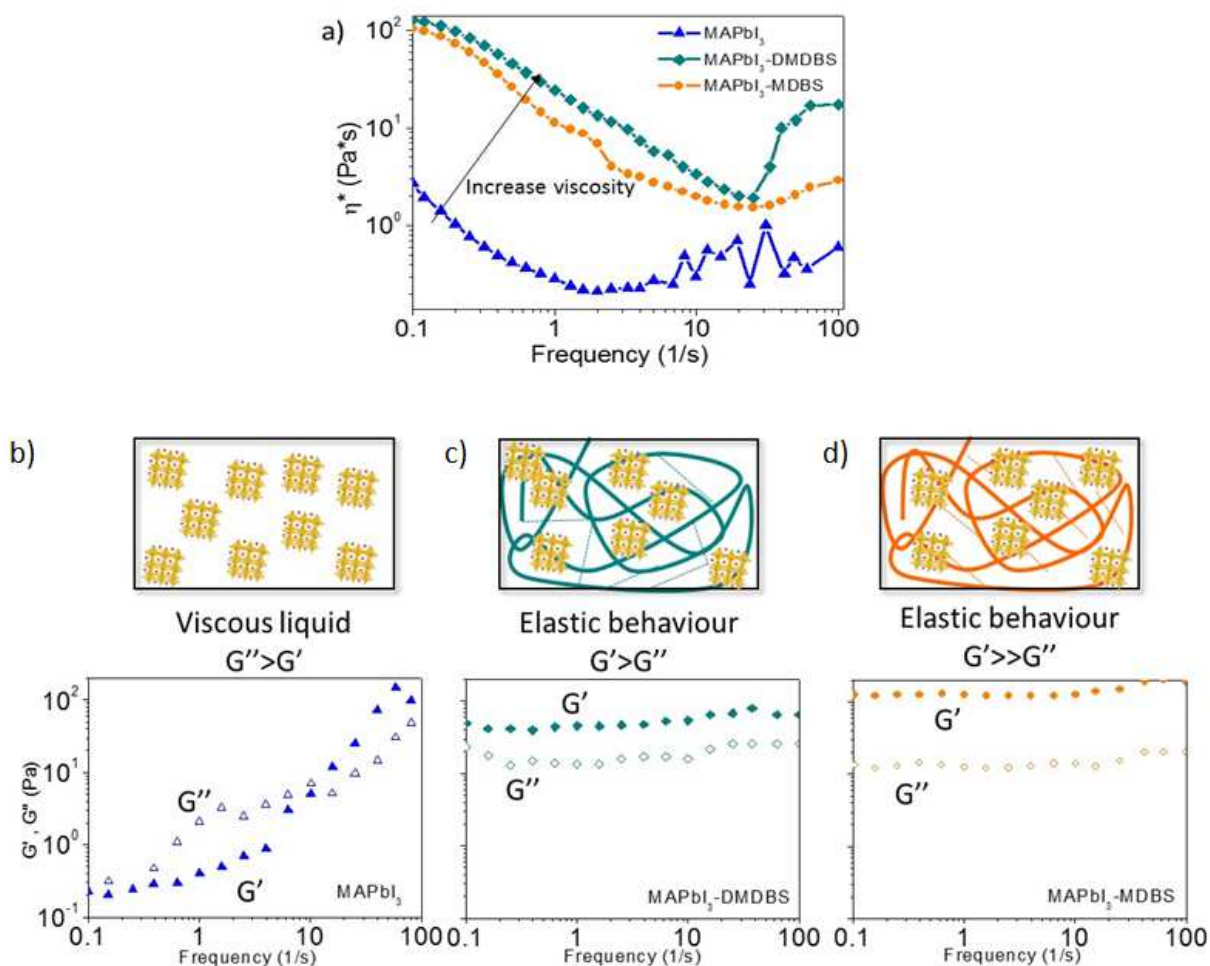


Figure 3. 2D-intensity maps during film formation from (a) the pristine perovskite precursor solution, and (b,c) solutions comprising 0.1 wt% (b) and 0.5 wt% MDBS (c), respectively. Dripping time variations of 5 seconds and less fall within the experimental error of the measurements and was found not to affect device performance. Individual q -plots taken at (d) $t = 15$ s, (e) $t = 30$ s, (f) $t = 45$ s and (g) $t = 90$ s. Insets of (e)-(g) focus on the $8 < q < 11$ nm⁻¹ range.

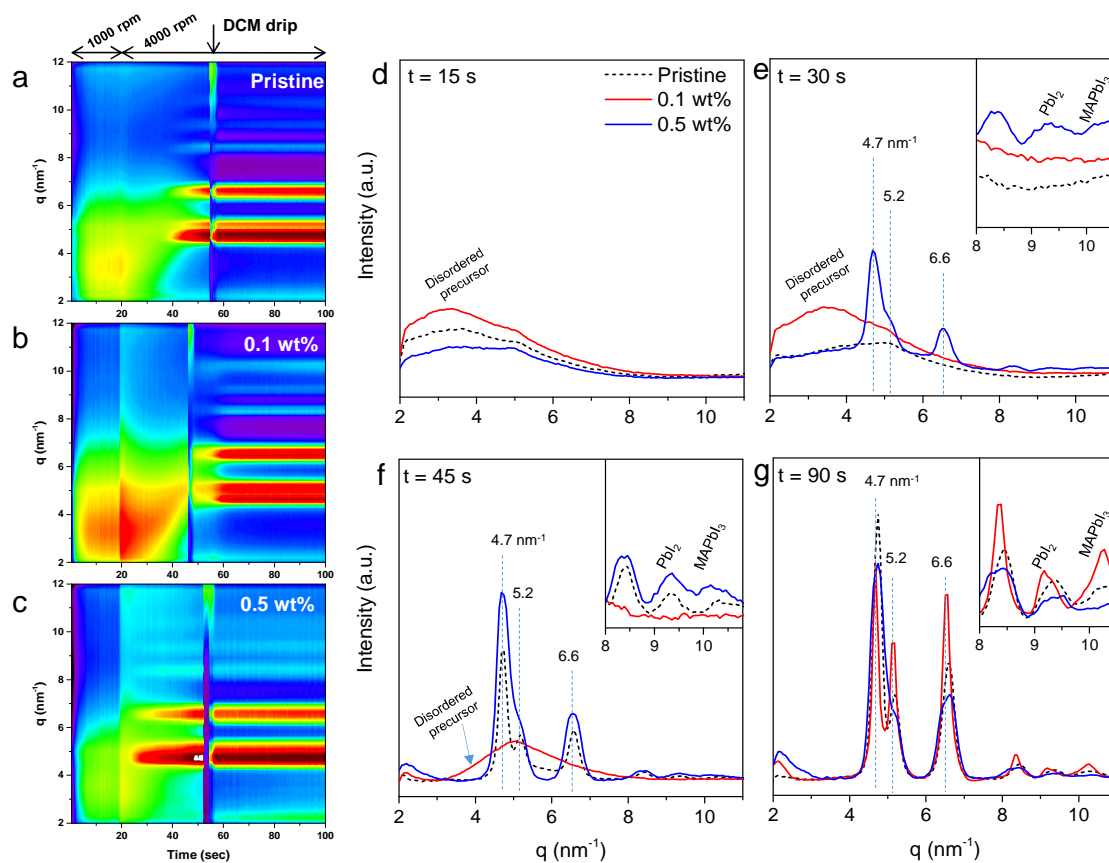


Figure 4. Optical micrographs taken at increasing temperatures of films prepared from pristine perovskite solutions and solutions comprising 0.1 wt% MDBS and 0.5 wt% MDBS.

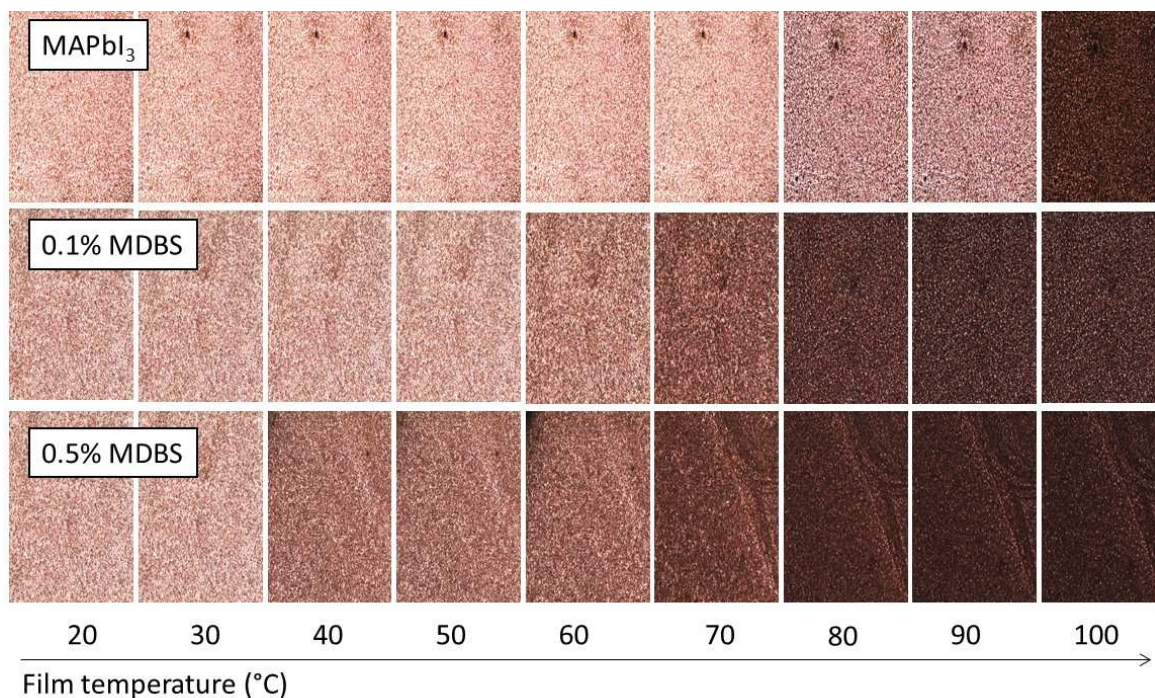


Figure 5. (a) DSC thermograms, where the endothermic peak related to the solvent evaporation has been subtracted in order to isolate the perovskite crystallization exotherm of pristine MAPbI₃ solutions and systems where 0.1 wt% of MDBS was added. (b) Enthalpy diagram of perovskite crystallization with and without MDBS.

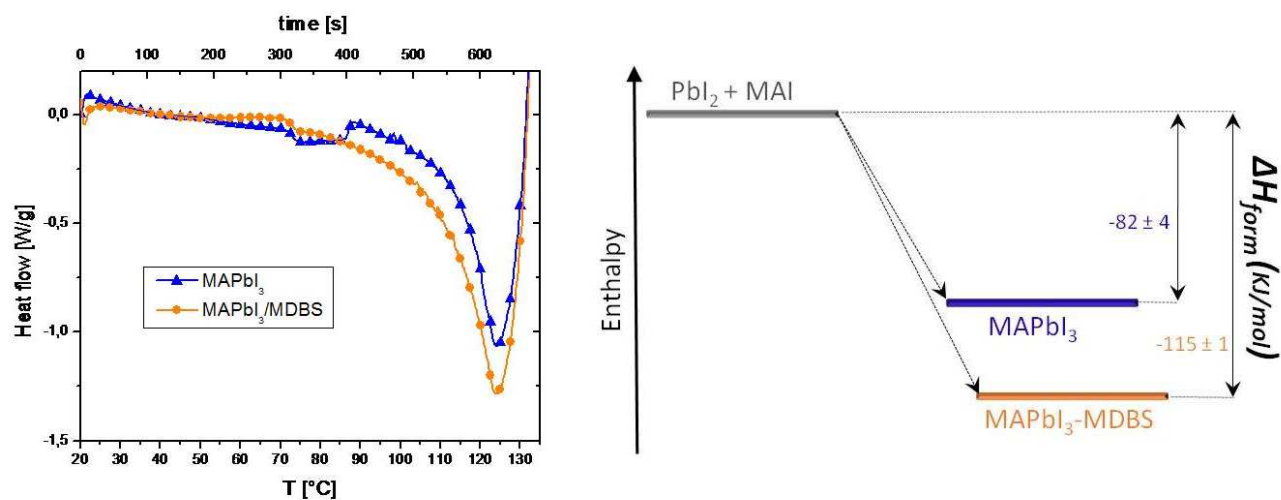


Figure 6. (a) SEM top view of films prepared with pristine perovskite precursor solutions and solutions comprising 0.1 wt% MDBS. TiO₂ substrates were used for this purpose. (b) Uv-vis absorption spectra of such films; (c) Current–voltage characteristics for champion devices prepared without (blue) and with 0.1 wt% MDBS (orange). The devices were measured under AM 1.5 at one sun. (d) SEM cross-sections of corresponding devices to which a schematic of the photovoltaic device architecture is overlaid.

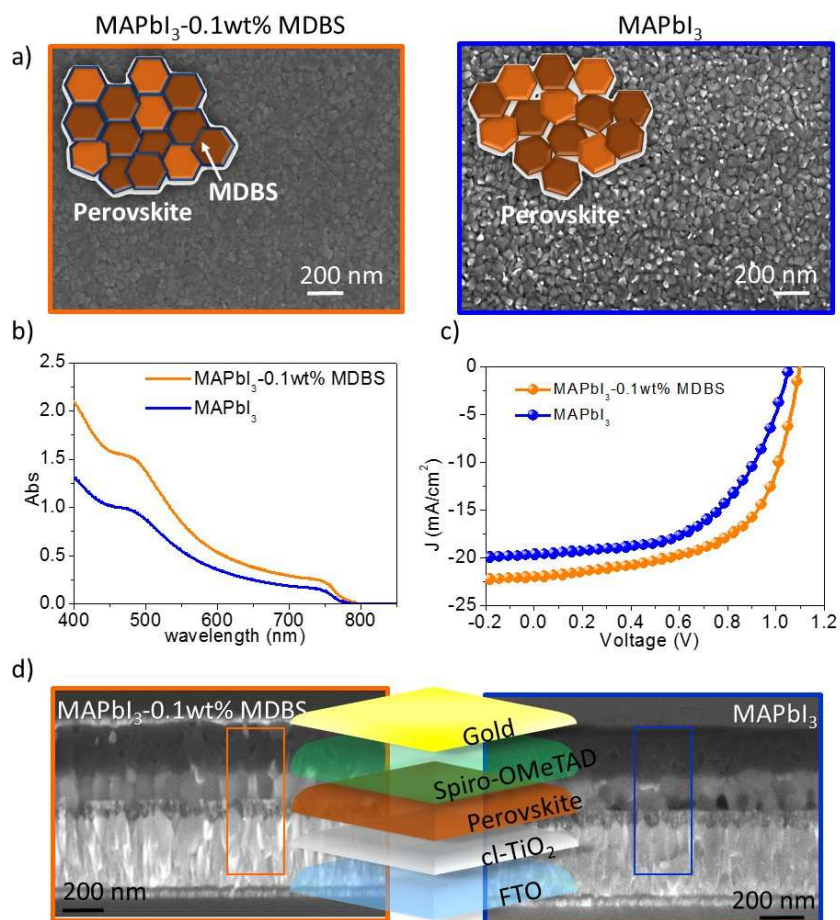


Table 1. Integrated intensities and FWHM of the diffraction features recorded for MDBS-based systems

Pristine					0.1 wt%					0.5 wt%				
Peak nm ⁻¹	FWHM / nm ⁻¹ (Integrated intensity / cts)				Peak nm ⁻¹	FWHM / nm ⁻¹ (Integrated intensity / cts)				Peak nm ⁻¹	FWHM / nm ⁻¹ (Integrated intensity / cts)			
	30s	45s	60s	90s		30s	45s	60s	90s		30s	45s	60s	90s
4.7	-	0.24 (91)	0.26 (189)	0.26 (212)	4.7	-	-	0.19 (64)	0.18 (106)	4.7	0.4 (119)	0.41 (230)	0.44 (281)	0.44 (287)
5.2	-	0.32 (29)	0.45 (103)	0.42 (106)	5.2	-	-	0.22 (51)	0.21 (92)	5.2	-	-	-	-
6.6	-	0.31 (42)	0.35 (109)	0.35 (116)	6.6	--	-	0.24 (98)	0.23 (117)	6.6	0.37 (40)	0.45 (96)	0.51 (132)	0.4 (196)
9.4	-	0.39 (3.2)	0.5 (8.6)	0.75 (17.4)	9.4	-	-	0.57 (5)	0.54 (7.6)	9.4	-	0.48 (9)	0.57 (8.4)	13 (0.7)
10.3	-	0.98 (7.6)	0.53 (6.9)	0.54 (6.3)	10.3	-	-	0.38 (14.8)	0.38 (13)	10.3	1.1 (7.8)	1.1 (4.7)	1.1 (4.7)	0.7 (1.1)

Table 2. Figure of merit of devices fabricated from solutions comprising varying amounts of MDBS: open-circuit voltage (V_{oc}), short-circuit current density (J_{sc}), fill factor (FF), and PCE.

	V_{oc} (V)	J_{sc} (mA/cm ²)	FF	PCE
MAPbI ₃	1.06	20.0	0.56	11.5
MAPbI ₃ /0.1 wt%-MDBS	1.10	22.0	0.60	14.5
MAPbI ₃ /0.5 wt%-MDBS	0.94	19.6	0.52	9.6

The table of content

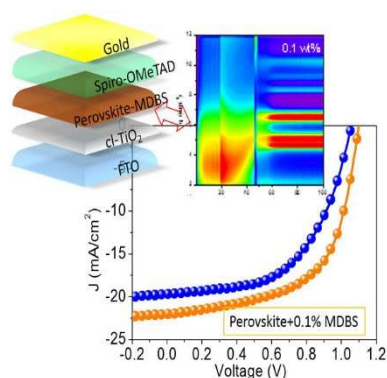
Organic gelators, widely used in the processing of commodity ‘plastics’, are applied here to hybrid halide perovskites solidification. They are shown to beneficially influence the nucleation and growth of the perovskite precursor phase, leading to a material characterized by a higher stability to moisture and a reduced hysteresis in planar n-i-p heterojunction solar cells.

Organic gelators as growth control agents for stable and reproducible hybrid perovskite-based solar cells

Keywords: halide perovskites, organic gelators, photovoltaics

Sofia Masi, Aurora Rizzo, Rahim Munir, Andrea Listorti, Antonella Giuri, Carola Esposito

Corcione, Neil Treat, Giuseppe Gigli, Aram Amassian, Natalie Stingelin, and Silvia Colella



Copyright WILEY-VCH Verlag GmbH & Co. KGaA, 69469 Weinheim, Germany, 2016.

Supporting Information

Organic gelators as growth control agents for stable and reproducible hybrid perovskite-based solar cells

Sofia Masi, Aurora Rizzo, Rahim Munir, Andrea Listorti, Antonella Giuri, Carola Esposito Corcione, Neil Treat, Giuseppe Gigli, Aram Amassian, Natalie Stingelin,* and Silvia Colella**

Figure S1. (a) Pictures of MDDBS and DMDBS 0.5 wt% solution in γ -BL:DMSO 2:1; (b) SEM top view of MAPbI₃ + 0.1wt% DMDBS film on TiO₂ substrate.

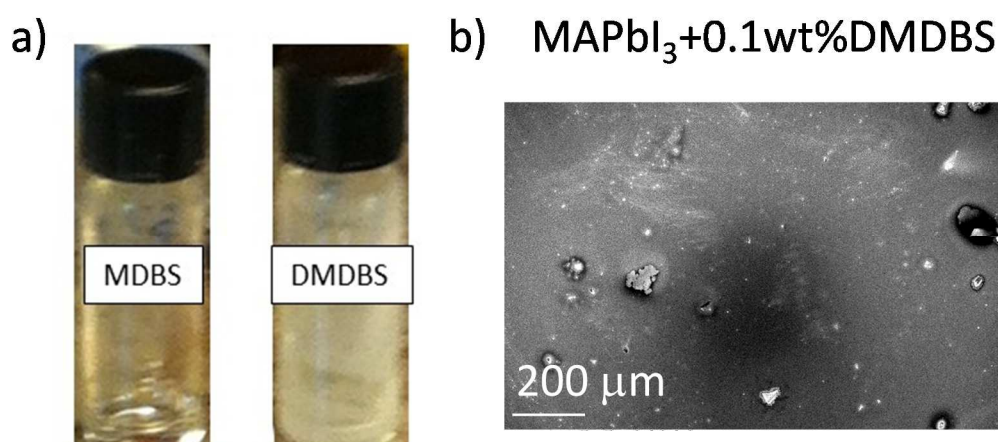


Figure S2. Comparison of the storage (G') and loss modulus (G'') profile versus frequency for a) MDDBS 0.1 wt% and MAPbI₃ + 0.1 wt% MDDBS and b) for DMDBS 0.1 wt% and MAPbI₃ + 0.1 wt% DMDBS solutions.

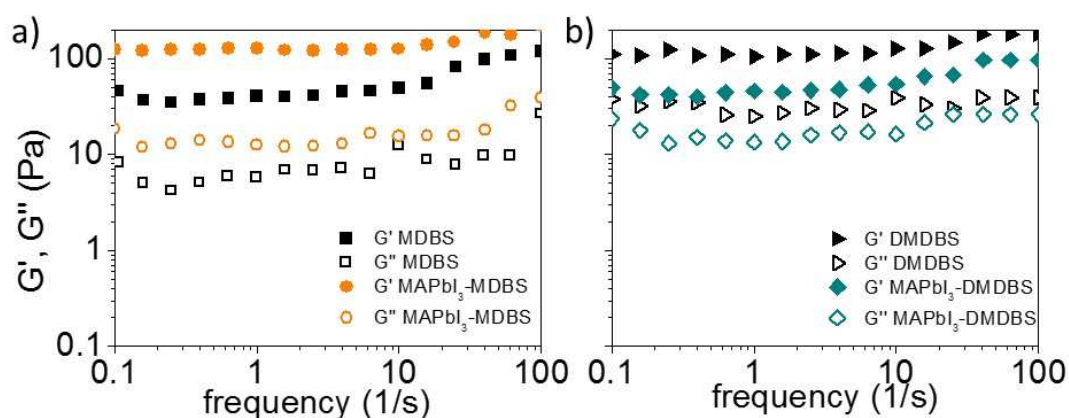


Figure S3. Two-dimensional GIWAXS images taken at key moments ($t = 15, 30, 45$ and 90 s) after initiating the spin-coating of the pristine solution.

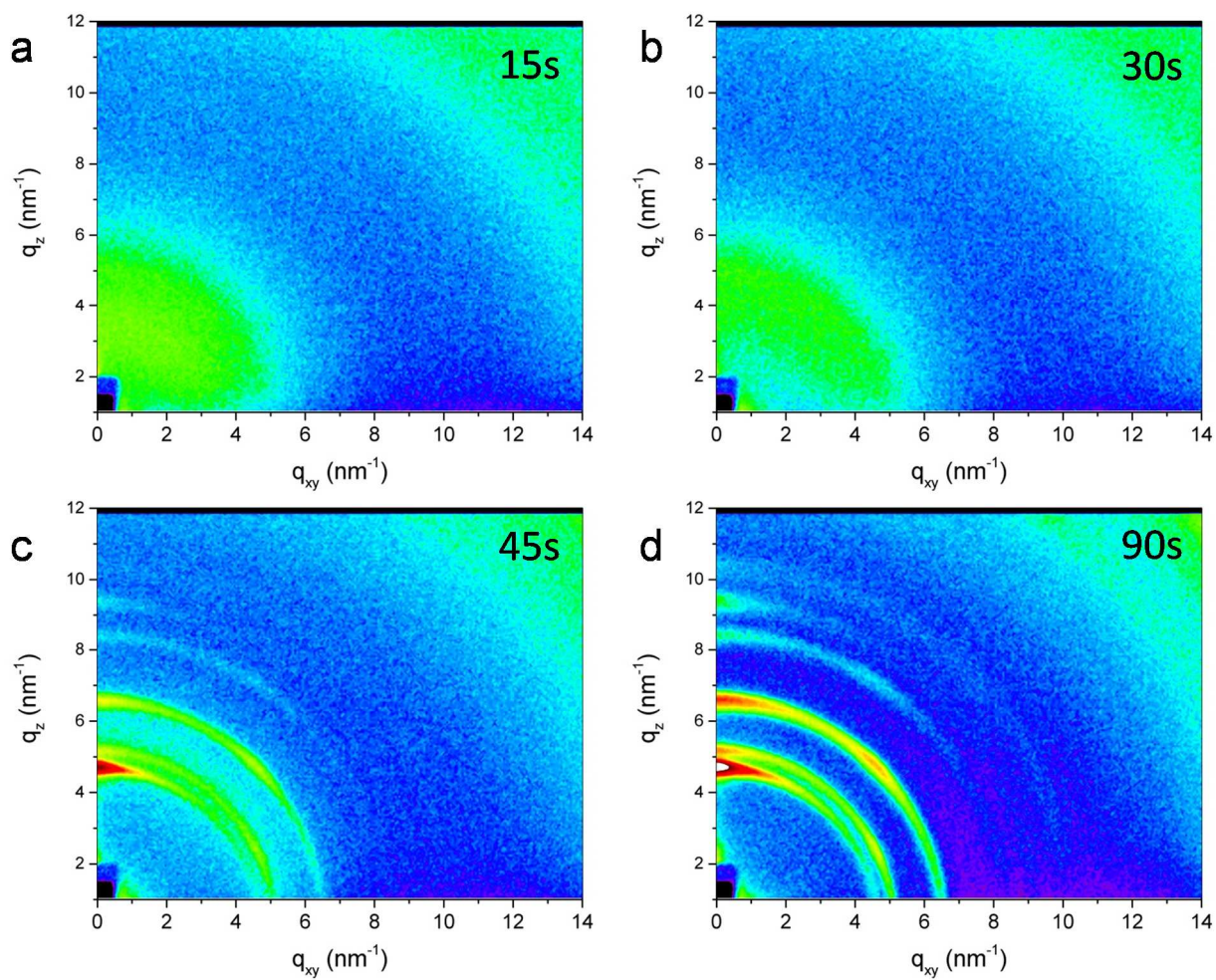


Figure S4. Two-dimensional GIWAXS image of pristine sample showing the cake integration performed on each GIWAXS image.

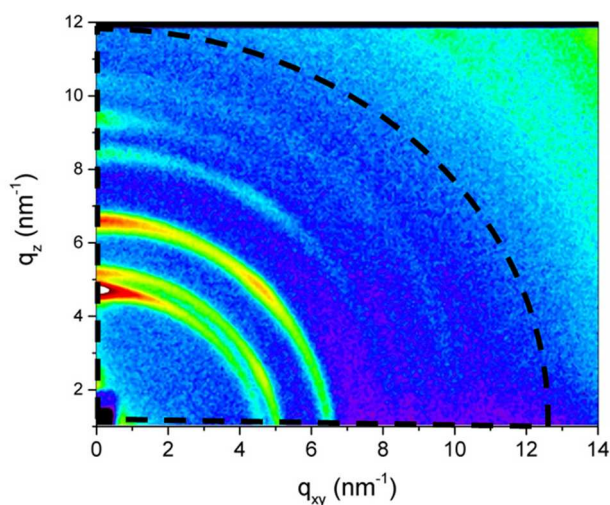


Table S1. Differential scanning calorimetry (DSC) parameters: starting (T_{onset}) peak (T_{peak}) and ending (T_{endset}) temperatures at different scan rate ($^{\circ}\text{C}/\text{min}$) for MAPbI_3 , $\text{MAPbI}_3/0.1$ wt% MDDBS and $\text{MAPbI}_3/0.1$ wt% DMDBS. The formation enthalpy (ΔH) has the same value for each scan rate.

Sample	Scan rate $^{\circ}\text{C}/\text{min}$	T_{onset} ($^{\circ}\text{C}$)	T_{peak} ($^{\circ}\text{C}$)	T_{endset} ($^{\circ}\text{C}$)	$t_{\text{endset}}-t_{\text{onset}}$ (s)	ΔH (kJ/mol)
MAPbI ₃	0.5	64	70	75	1,306	82 ± 4
	2	84	95	100	414	
	5	99	111	117	209	
	10	111	124	131	123	
MAPbI ₃ +MDDBS 0.1wt%	0.5	60	70	75	1,824	115 ± 1
	2	80	92	99	556	
	5	95	110	116	252	
	10	103	124	132	161	
MAPbI ₃ +DMDBS 0.1wt%	0.5	64	72	75	1,274	72 ± 13
	2	83	93	99	474	
	5	98	110	116	209	
	10	112	124	131	116	

Figure S5. (a) Comparison of the storage modulus (G') at different temperature of bare perovskite solution, perovskite + 0.1 wt% MDDBS solution and perovskite + 0.1 wt% DMDDBS solution, at 1 Hz. G' values are taken at 1Hz from the elastic storage (G') versus frequency scans, at different temperatures, of (b) bare perovskite solution, (c) perovskite + 0.1 wt % MDDBS solution and (d) perovskite + 0.1 wt % DMDDBS solution.

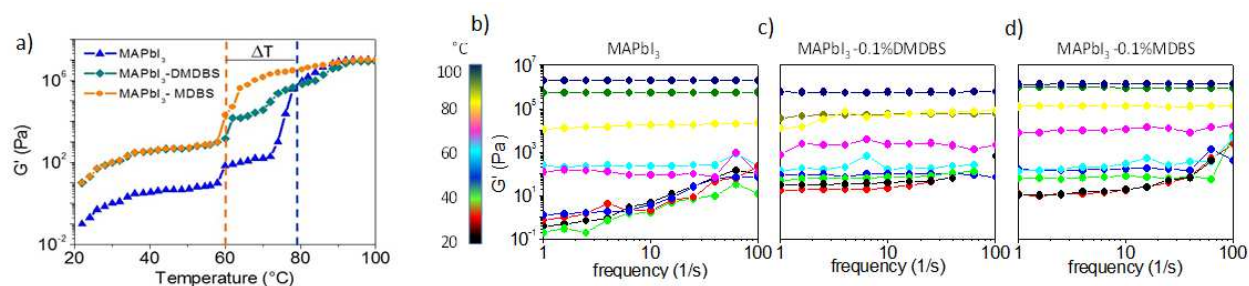


Figure S6. XRD patterns of films produced from a neat precursor solution (left) compared to structures that were produced with 0.1 wt% MDDBS. A comparison is shown of as prepared and aged films kept 15 day in ambient conditions, at 70 % humidity.

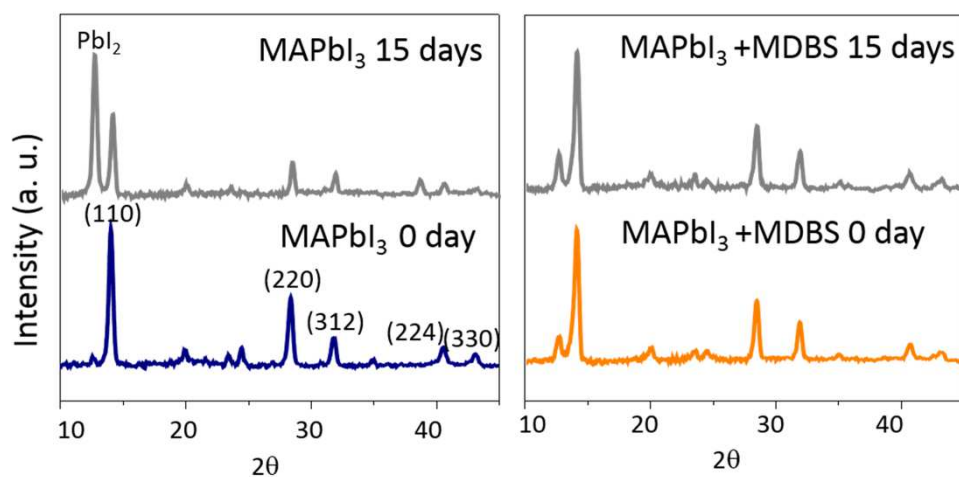


Table S2. Solar cell figures of merit of devices fabricated with varying amounts of DMDBS incorporated into casting solution

	PCE (%)	FF	Voc (V)	Jsc(mA/cm ²)	Mean \pm s.d.
MAPbI ₃ -DMDBS 0.1 wt%	0.7	0.28	0.61	4.0	0.7 \pm 0.2
MAPbI ₃ -DMDBS 0.5 wt%	0.3	0.17	0.68	2.6	0.3 \pm 0.1

Table S3. Main photovoltaic parameters of cells using perovskite and perovskite-MDBS, measured by forward and reverse scans to calculate the hysteresis index.^[1]

	PCE (%)	FF	Voc (V)	Jsc (mA/cm ²)	Hysteresis index
With MDBS Reverse	15.0	0.64	1.08	21.8	0.03
With MDBS Forward	14.5	0.60	1.1	22.0	
w/o MDBS Reverse	8.5	0.45	1.1	17.6	0.09
w/o MDBS Forward	11.5	0.56	1.06	20	

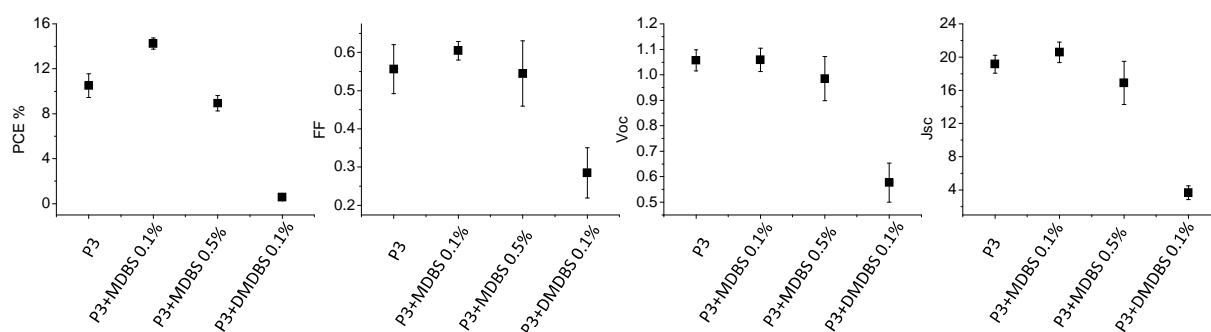
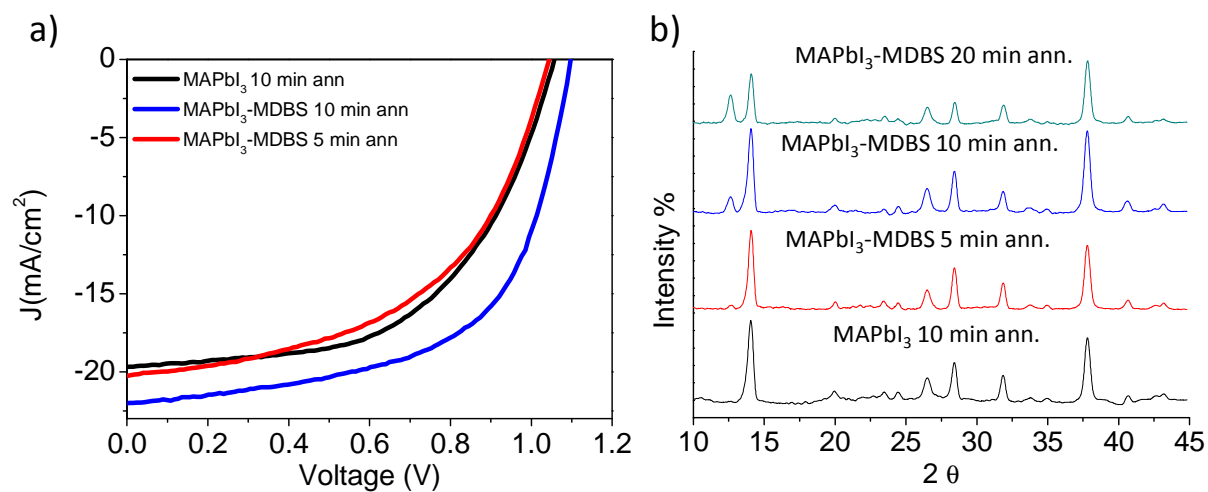
Figure S7. Statistics of PCE (%), FF, Voc and Jsc of devices based on perovskite and perovskite with different amount of MDBS layers.

Figure S8. (a) J-V curves of device based on bare perovskite and device based on perovskite-MDBS 0.1 wt% at different annealing time; (b) corresponding XRD patterns.



[1] R. S. Sanchez, V. Gonzalez-Pedro, J.-W. Lee, N.-G. Park, Y. S. Kang, I. Mora-Sero, J. Bisquert, *The Journal of Physical Chemistry Letters* **2014**, 5 (13), 2357-2363.